Localized States in Active Fluids

Luca Barberi[1,2,*] and Karsten Kruse[1,2,3,†]

[1]*Department of Biochemistry, University of Geneva, 1211 Geneva, Switzerland*
[2]*Department of Theoretical Physics, University of Geneva, 1211 Geneva, Switzerland*
[3]*NCCR for Chemical Biology, University of Geneva, 1211 Geneva, Switzerland*

Biological active matter is typically tightly coupled to chemical reaction networks affecting its assembly-disassembly dynamics and stress generation. We show that localized states can emerge spontaneously if assembly of active matter is regulated by chemical species that are advected with flows resulting from gradients in the active stress. The mechanochemical localized patterns form via a subcritical bifurcation and for parameter values for which patterns do not exist in absence of the advective coupling. Our work identifies a generic mechanism underlying localized cellular patterns.

Chemical reactions can lead to the emergence of patterns, that is, spatiotemporally structured densities of the chemical species involved [1]. Active materials that transform chemical energy into mechanical work can self-organize flow patterns and shapes [2]. Systems coupling these two forms of self-organization are widespread, notably in engineering and biology. Typically, in these systems, chemistry is considered to control the mechanical parts. Yet, researchers increasingly focus on situations where chemistry and mechanics are mutually affecting each other [3,4]. Despite the growing interest in these systems, our understanding of spontaneous mechanochemical patterns is still limited.

A particularly interesting example of a biological mechanochemical system is the actin cortex of animal cells. It is a thin active layer beneath the outer membrane and consists of actin filaments, myosin motors, and other actin-binding proteins. It exhibits a variety of spatiotemporal patterns, some of which have been argued to result from self-organization during vital cellular processes like migration [5–7] or development [8–10]. The implications of mechanochemistry in the dynamics of the actin cortex are currently under intense theoretical scrutiny [11–15].

Whereas the most studied patterns extend over the whole cell surface, the actin cortex also exhibits localized structures. Examples of the latter are isolated contractions, either transient [16] or oscillatory [17], observed in adherent cells, as well as isolated clusters of actin and signaling molecules in cancer cells [18,19].

The mechanism underlying the localized structures mentioned above has not yet been theoretically addressed. Here, we argue that these structures correspond to localized states (LSs) of spatially extended dynamical systems, i.e., self-organized states where a background state—here, the homogenous, isotropic cortex—remains essentially unaffected except in a finite region of space. In integrable

systems, LSs are well known, for instance in the form of solitons, but they also occur in dissipative systems [20]. However, they have not been reported for the actin cortex or, generally, active fluids.

Specifically, we use a continuum description to show that mechanochemistry can produce self-organized LSs in active fluids. Our description accounts for a generic activator-inhibitor circuit involved in actin assembly [6,17,21,22], as well as for convective flows induced by gradients in the active stress [2].

Consider an isotropic active fluid. Its state is given by the density c of the actomyosin network. The time evolution of c is captured by the continuity equation

$$\partial_t c + \nabla \cdot \boldsymbol{j}_c = \alpha n_a - k_d c, \qquad (1)$$

where ∇ is the spatial gradient operator, and the current $\boldsymbol{j}_c = c\boldsymbol{v} - D_c \nabla c$. The current consists of a convective and a diffusive part, where the latter accounts for fluctuations in the system through the effective diffusion constant D_c. Since cortical dynamics occurs at low Reynolds number, we neglect inertial effects, such that the fluid velocity $\boldsymbol{v}$ is determined by force balance,

$$\nabla \cdot \sigma = \gamma \boldsymbol{v}, \qquad (2)$$

$$\sigma = 2\eta \mathsf{v} + \tilde{\eta} \nabla \cdot \boldsymbol{v} \mathbb{1} + \pi(c). \qquad (3)$$

Here, σ denotes the stress tensor and γ is a constant with the dimensions of a friction coefficient that captures dissipation in the cortex resulting, for example, from friction between the actin network and the cell membrane.

The stress tensor has a viscous component, where η and $\tilde{\eta}$, respectively, denote the shear and bulk viscosity of the active fluid, $\mathsf{v} = (1/2)[\nabla\boldsymbol{v} + (\nabla\boldsymbol{v})^T - (\nabla \cdot \boldsymbol{v}/d)\mathbb{1}]$ is the traceless strain rate tensor, d the number of spatial

dimensions, and $\mathbb{1}$ is the identity. The nonviscous component, $\pi(c) = [\pi_a(c) + \pi_p(c)]\mathbb{1}$, includes active and passive terms, $\pi_a(c) = (\zeta\Delta\mu)_0 c^2$ and $\pi_p(c) = -bc^3$, respectively. We assume the stress to be contractile for small densities c, $(\zeta\Delta\mu)_0 > 0$, whereas for high densities the hydrostatic contribution dominates, $b > 0$ [23].

The remaining terms in Eq. (1) are discussed in Ref. [24] and describe the effects of actomyosin assembly and disassembly. In the actin cortex, assembly is mediated by active actin nucleators [25,26], whose density is n_a.

The actin cytoskeleton and the network regulating its assembly and activity form an excitable medium [17,21,22]. We account for this feature in terms of a generic activator-inhibitor model [24,27]. Explicitly,

$$\partial_t n_a + \nabla \cdot \boldsymbol{j}_a = \omega_0(1 + \omega n_a^2)n_i - (\omega_{d,0} + \omega_d c)n_a, \quad (4)$$

$$\partial_t n_i + \nabla \cdot \boldsymbol{j}_i = -\omega_0(1 + \omega n_a^2)n_i + (\omega_{d,0} + \omega_d c)n_a, \quad (5)$$

where n_i is the distribution of inactive nucleators. In addition to diffusion with respective diffusion constants D_a and D_i, active and inactive nucleators are advected with the active fluid, such that $\boldsymbol{j}_a = n_a \boldsymbol{v} - D_a \nabla n_a$ and analogously for the inactive nucleators. We take $D_i \gg D_a$, because, in cells, inactive nucleators are cytosolic, whereas active ones are membrane bound [25]. All terms on the right hand side of Eqs. (4) and (5) are discussed in Ref. [24], except for the spontaneous inactivation rate $\omega_{d,0}$. Note that they conserve the total average nucleator density, $\bar{n} = (1/\mathcal{V})\int_\mathcal{V}(n_a + n_i)d\mathcal{V}$, where $\mathcal{V}$ is the system volume. Below, we consider periodic boundary conditions. No-flux boundary conditions do not change our results.

We first consider the case of one spatial dimension, $d = 1$, with $x \in [-l/2, l/2]$. For simplicity, we assume that $\eta = \tilde{\eta}$. We introduce nondimensional variables, where the unit length is $\lambda = \sqrt{\eta/\gamma}$, the typical distance over which the velocity field decays due to viscosity and friction, and the unit time is $\tau = \lambda^2/D_i$, the typical time taken by an inactive nucleator to diffuse a distance λ. Furthermore, densities are scaled by $\bar{n}$. We denote nondimensional quantities with capital letters: $X = x/\lambda$, $T = t/\tau$, $C = c/\bar{n}$, $N_{a(i)} = n_{a(i)}/\bar{n}$, and so on, Supplemental Material (SM), Table II [28].

We first consider the case $\Omega_{d,0} = 0$. In this case, Eqs. (1)–(5) have a unique homogenous steady state (H) [24]. A linear stability analysis shows that this state can become unstable in favor of heterogeneous states that span the whole system, through finite wavelength stationary or oscillatory (type I_s or type I_o [29]) instabilities, SM Sec. I [28]. Note that the conservation of $\bar{n}$ implies a neutrally stable (large-scale) mode of the dynamics, SM Sec. I [28]. We obtain heterogenous states by solving Eqs. (1)–(5) numerically. To this end, we use a custom Julia [30] code, available online [31].
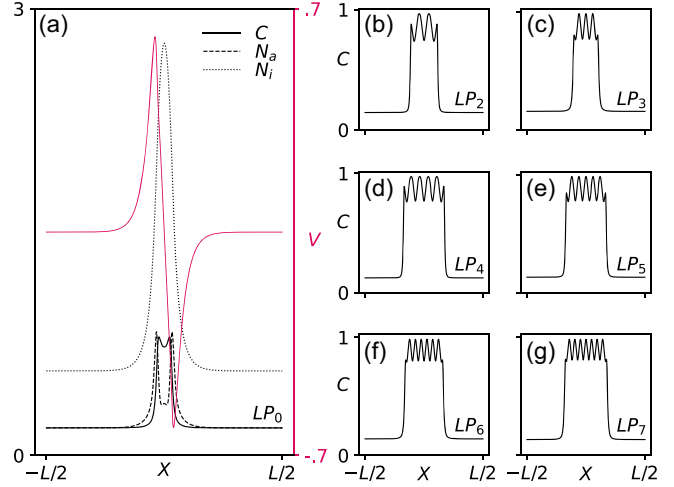

FIG. 1. Localized patterns (LPs). (a) Density (black lines) and velocity (pink line) profiles of a LP without internal peaks, LP_0. (b)–(g) Multipeaked LP_i, where $i = 2, \dots, 7$ is the number of internal peaks. Parameter values as in SM Table II [28], with $\Omega_{d,0} = 0$, $\Omega_d = 10$, $Z = 15$, and $\Omega = 6$ (a), 10 (b),(c), 14 (d)–(f), 15.5 (g).

In addition to patterns spanning the whole system, our numerical solutions reveal a rich variety of stable localized patterns (LPs). LPs are a specific class of LSs that exhibit some internal structure and typically come in groups of related and (partially) coexisting states. In our system, LPs feature an increased active fluid and nucleator density in a confined region, Fig. 1(a). Outside this region, the densities rapidly decay to some limiting values. With increasing system size, the high density profiles converge and the densities outside approach H, SM Fig. 3 [28]. Asymptotic convergence and lateral decay to H classifies these states as localized [20,32]. The parameter region where LPs exist changes with increasing system size, but eventually converges to a domain of finite measure [33,34].

The corresponding velocity profile indicates a constant flow into the high density region, Fig. 1(a). In addition, there is net assembly at the borders of the high-density region, SM Fig. 4 [28]. These processes are compensated by diffusive outflux from and disassembly in the center, SM Fig. 4 [28].

Additional LPs exhibit internal patterns with different numbers of density maxima (peaks), Figs. 1(b)–1(g). The internal patterns can be understood as a consequence of an instability of H. This idea was used in Refs. [35,36], when studying localized patterns in reaction-diffusion systems subject to inhomogeneous forcing. Here, the homogenous state H is the one of Eqs. (1)–(5) with the total nucleator density $\bar{n}$ equal to that in the high density region of the states LP_2 to LP_7 and all other parameters unchanged, SM Sec. I [28]. Even though the linear stability analysis indicates that the system is far away from the bifurcation, the characteristic length of the LP in the high density region falls well into the interval of linearly unstable modes.
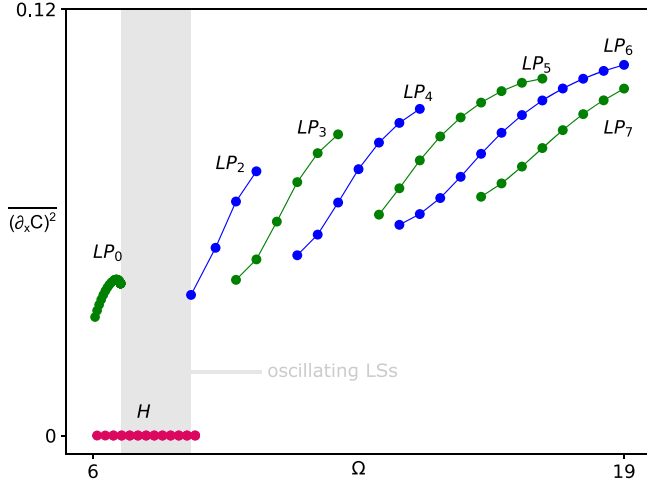
FIG. 2. Slanted snaking. Bifurcation diagram of localized patterns (LPs). Unstable branches are not shown. In the gray-colored region, LP_0 loses stability to oscillatory localized states. $\overline{(\partial_X C)^2} = (1/L) \int_{-L/2}^{L/2} (\partial_X C)^2 dX$. Parameters and labels as in Fig. 1.
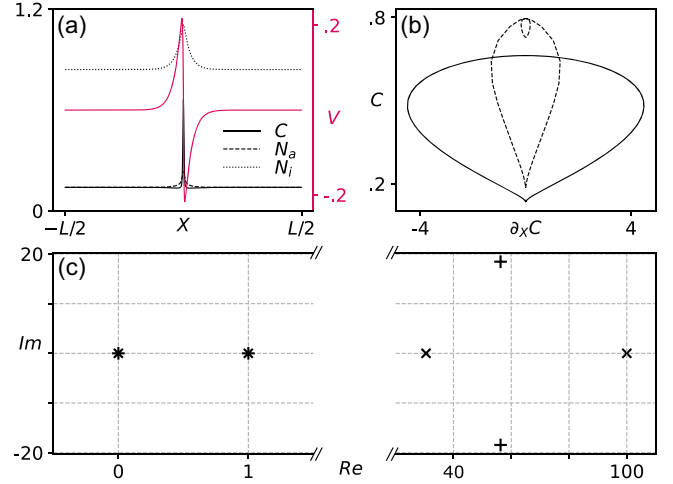

FIG. 3. Spikes vs localized patterns (LPs). (a) Profile of a spike. Parameter values as in SM Table II [28], with $\Omega = 0$, $\Omega_{d,0} = 3$, $\Omega_d = 0$, $Z = 20$. (b) Spatial dynamics' orbits corresponding to the spike in panel (a), solid line, and LP_0 in Fig. 1(a), dashed line, projected onto the $(C, dC/dX)$ plane. (c) Eigenvalues of the spatial dynamics linearized around H, for parameter values corresponding to the spike in panel (a), $\times$, and LP_0, $+$. In either case, the eigenvalue with real part equal to 1 has multiplicity 4. To facilitate the view, the horizontal axis is broken and its scale changes from left to right.

The velocity profile indicates a permanent convective outflow from the internal peaks, SM Fig. 5 [28]. This enables a repulsive hydrodynamic interaction between neighboring peaks, which stabilizes LPs [37]. Active fluid peaks are chemically maintained by nucleation through corresponding internal peaks of active nucleator density, SM Fig. 5 [28]. These in turn are maintained by a permanent diffusive inflow of inactive nucleators that locally activate, SM Fig. 5 [28]. This structure is in line with the linear stability analysis and confirms that LPs are mechanochemical in nature instead of resulting from a chemical instability.

Equations (1)–(5) belong to the broad class of localized-pattern forming systems exhibiting snaking, with examples in chemistry, hydrodynamics, and optics [20,34]. Indeed, the bifurcation diagram of LPs, Fig. 2, reveals a slanted snaking scenario [38,39], typical of systems featuring a finite-wavelength instability and a large-scale mode. In slanted snaking, LPs with an even and odd number of internal peaks form two, separate, intertwined branches (whence the name "snaking").

In our mechanochemical system, localization does not require nonlinear chemical reactions. Consider the linear kinetics limit of Eqs. (4) and (5), with $\Omega = \Omega_d = 0$. In this limit, the system admits LSs in the form of spikes [40] that do not have internal patterns (peaks), Fig. 3(a). The absence of LPs in this regime shows that the internal patterns of the states in Figs. 1(b)–1(g) and SM Fig. 5 [28] strictly rely on cooperative nucleator activation.

To clarify the nature of LPs and spikes as well as the transition from one to the other, we employ spatial dynamics [41,42]. That is, we consider the stationary version of Eqs. (1)–(5) and interpret the spatial

coordinate X as a (fictitious) time. We end up with eight coupled ordinary differential equations for the effective coordinates (C, N_a, N_i, V) and their effective conjugated momenta $P_C = dC/dX$, $P_a = dN_a/dX$, $P_i = dN_i/dX$, $P_V = dV/dX$, SM Sec. II [28]. The spatial dynamic system is reversible, i.e., symmetric for $(X, V) \to (-X, -V)$.

The homogenous stationary state H of the full dynamic equations corresponds to a fixed point of the spatial dynamics. In an infinite system, $L = \infty$, LSs map to homoclinic orbits joining H to itself in the spatial dynamics, Fig. 3(b). These lie on the intersection of the stable and unstable manifolds of H with points on the stable manifold evolving toward H as $X \to \infty$, whereas points on the unstable manifold reach it for $X \to -\infty$. If the evolution toward and away from the fixed point is monotonic, the homoclinic orbit corresponds to a spike in the full dynamical system. Otherwise, it corresponds to an LP. This distinction can be captured by the eigenvalues of the spatial dynamics linearized around H: spikes correspond to real and LPs to complex spatial eigenvalues, Fig. 3(c). Note that eigenvalues come in complex-conjugate pairs, due to reversibility [34]. The transition from a complex-conjugate pair (LP) to two real eigenvalues (spike) is reminiscent of a Belyakov-Devaney instability [32,40].

LSs persist in two spatial dimensions (2D). Consider a square domain, $(x, y) \in [-l/2, l/2] \times [-l/2, l/2]$, with periodic boundaries. In 2D, we find LPs with circular, Figs. 4(a) and 4(b), or band-shaped domains, Figs. 4(c) and 4(d). In either case, the velocity profile indicates a
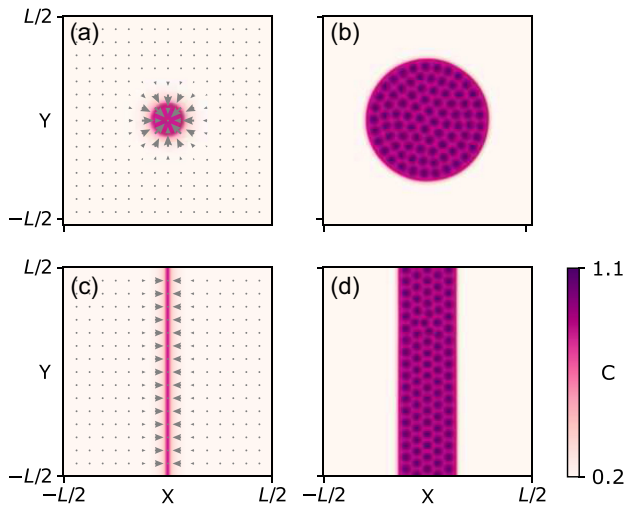
FIG. 4. Localized states in 2D. (a),(b) Isotropically localized states, simple (a) and patterned (b). (c),(d) Anisotropically localized states, simple (c) and patterned (d). Arrows represent velocity fields (a),(c). Parameters as in SM Table II [28], with $\Omega_{d,0} = 0$, $Z = 30$, and $\Omega = 0$ (a),(c), $\Omega = 9$ (b),(d). The code used to obtain these results is available online [31].

constant flow into the high-density region, Figs. 4(a) and 4(c). LSs with different symmetries can coexist, in which case the steady state depends on the initial conditions. Both circular and band-shaped LSs can develop internal patterns, in the form of closely packed spots, Figs. 4(b) and 4(d). The velocity profile indicates a constant convective outflow from inner spots, SM Fig. 6 [28], similar to the 1D case.

To conclude, motivated by the actin cortex of animal cells, we studied a generic description of an active fluid coupled to an assembly regulating module and found a spectrum of LSs. In 1D, we could identify slanted snaking to be at the origin of stationary LPs. Some LSs bifurcate into oscillating LSs, which will be presented elsewhere.

In reversible systems, homoclinic orbits to hyperbolic fixed points are structurally stable [32,43], such that they are independent of the details of the underlying dynamic equations. In the system studied here, the fixed point H is not hyperbolic, due to the conservation of nucleators. Note, however, that its center manifold is physically inaccessible during the dynamics. Hence, from a physics standpoint, H should behave as a hyperbolic fixed point. Indeed, our LSs do not rely on parameter fine tuning or the presence of chemical nonlinearities, which is consistent with structural stability.

It has been argued that noise can promote transient LSs in reaction-diffusion signaling networks in the absence of mechanics [44]. Like localized extracellular stimuli, these might serve as prepatterns and trigger the mechanochemical route to stable LSs discussed above. Note that, in parameter regions where H is unstable, our system can generate LSs in the absence of a localized initial condition.

Because of the generic character of our approach, we refrain from a detailed comparison with experiments. Still, we want to point out some qualitative analogies between the states discussed above and cellular localized structures. In breast cancer cells, invadopodia are actin-rich protrusions that are surrounded by a ring of active Rho-C [19]. Rho-C is a small GTPase that is involved in activating actin nucleation [45]. A similar distribution is observed in the LS of Fig. 1(a), where the active nucleator is depleted from the center of the LS, where actin density is high, and concentrates at the edges of the LSs by acquiring a two-peaked profile. Other actin-rich protrusions are known as podosomes in macrophages, where they often coassemble into rather circular podosome clusters [46]. The circular LP in Fig. 4(b) is reminiscent of such clusters.

Beyond invadopodia and podosome clusters, LSs could serve as programmable active stress foci to generate local membrane protrusions, like filopodia [47] and dendritic spines [48]. As a consequence, different experimental systems are available to test the mechanism discussed in this work.

---

[*]luca.barberi@unige.ch
[†]karsten.kruse@unige.ch

[1] A. J. Koch and H. Meinhardt, Biological pattern formation: From basic mechanisms to complex structures, Rev. Mod. Phys. **66**, 1481 (1994).

[2] M. C. Marchetti, J. F. Joanny, S. Ramaswamy, T. B. Liverpool, J. Prost, M. Rao, and R. A. Simha, Hydrodynamics of soft active matter, Rev. Mod. Phys. **85**, 1143 (2013).

[3] A. De Wit, Chemo-hydrodynamic patterns and instabilities, Annu. Rev. Fluid Mech. **52**, 531 (2020).

[4] A. Bailles, E. W. Gehrels, and T. Lecuit, Mechanochemical principles of spatial and temporal patterns in cells and tissues, Annu. Rev. Cell Dev. Biol. **38**, 321 (2022).

[5] M. G. Vicker, Reaction-diffusion waves of actin filament polymerization/depolymerization in dictyostelium pseudopodium extension and cell locomotion, Biophys. Chem. **84**, 87 (2000).

[6] O. D. Weiner, W. A. Marganski, L. F. Wu, S. J. Altschuler, and M. W. Kirschner, An actin-based wave generator organizes cell motility, PLoS Biol. **5**, 2053 (2007).

[7] L. Stankevicins, N. Ecker, E. Terriac, P. Maiuri, R. Schoppmeyer, P. Vargas, A.-M. Lennon-Duménil, M. Piel, B. Qu, M. Hoth, K. Kruse, and F. Lautenschläger, Deterministic actin waves as generators of cell polarization cues, Proc. Natl. Acad. Sci. U.S.A. **117**, 826 (2020).

[8] J. Solon, A. Kaya-Çopur, J. Colombelli, and D. Brunner, Pulsed forces timed by a Ratchet-like mechanism drive directed tissue movement during Dorsal closure, Cell **137,** 1331 (2009).

[9] A. Munjal, J.-M. Philippe, E. Munro, and T. Lecuit, A self-organized biomechanical network drives shape changes during tissue morphogenesis, Nature (London) **524,** 351 (2015).

[10] A. Bailles, C. Collinet, J.-M. Philippe, P.-F. Lenne, E. Munro, and T. Lecuit, Genetic induction and mechano-chemical propagation of a morphogenetic wave, Nature (London) **572,** 467 (2019).

[11] J. S. Bois, F. Jülicher, and S. W. Grill, Pattern formation in active fluids, Phys. Rev. Lett. **106,** 028103 (2011).

[12] A. Chaudhuri, B. Bhattacharya, K. Gowrishankar, S. Mayor, and M. Rao, Spatiotemporal regulation of chemical reactions by active cytoskeletal remodeling, Proc. Natl. Acad. Sci. U.S.A. **108,** 14825 (2011).

[13] K. V. Kumar, J. S. Bois, F. Jülicher, and S. W. Grill, Pulsatory patterns in active fluids, Phys. Rev. Lett. **112,** 208101 (2014).

[14] D. S. Banerjee, A. Munjal, T. Lecuit, and M. Rao, Acto-myosin pulsation and flows in an active elastomer with turnover and network remodeling, Nat. Commun. **8,** 1121 (2017).

[15] M. F. Staddon, E. M. Munro, and S. Banerjee, Pulsatile contractions and pattern formation in excitable actomyosin cortex, PLoS Comput. Biol. **18,** e1009981 (2022).

[16] M. A. Baird, N. Billington, A. Wang, R. S. Adelstein, J. R. Sellers, R. S. Fischer, and C. M. Waterman, Local pulsatile contractions are an intrinsic property of the myosin 2A motor in the cortical cytoskeleton of adherent cells, Mol. Biol. Cell **28,** 240 (2017).

[17] M. Graessl, J. Koch, A. Calderon, D. Kamps, S. Banerjee, T. Mazel, N. Schulze, J. K. Jungkurth, R. Patwardhan, D. Solouk, N. Hampe, B. Hoffmann, L. Dehmelt, and P. Nalbant, An excitable Rho GTPase signaling network generates dynamic subcellular contraction patterns, J. Cell Biol. **216,** 4271 (2017).

[18] M. Oser, H. Yamaguchi, C. C. Mader, J. Bravo-Cordero, M. Arias, X. Chen, V. DesMarais, J. van Rheenen, A. J. Koleske, and J. Condeelis, Cortactin regulates cofilin and N-WASp activities to control the stages of invadopodium assembly and maturation, J. Cell Biol. **186,** 571 (2009).

[19] J. J. Bravo-Cordero, M. Oser, X. Chen, R. Eddy, L. Hodgson, and J. Condeelis, A novel spatiotemporal RhoC activation pathway locally regulates cofilin activity at invadopodia, Curr. Biol. **21,** 635 (2011).

[20] E. Knobloch, Spatial localization in dissipative systems, Annu. Rev. Condens. Matter Phys. **6,** 325 (2015).

[21] W. M. Bement, M. Leda, A. M. Moe, A. M. Kita, M. E. Larson, A. E. Golding, C. Pfeuti, K.-C. Su, A. L. Miller, A. B. Goryachev, and G. von Dassow, Activator-inhibitor coupling between Rho signalling and actin assembly makes the cell cortex an excitable medium, Nat. Cell Biol. **17,** 1471 (2015).

[22] A. Michaud, M. Leda, Z. T. Swider, S. Kim, J. He, J. Landino, J. R. Valley, J. Huisken, A. B. Goryachev, G. von Dassow, and W. M. Bement, A versatile cortical pattern-forming circuit based on Rho, F-actin, Ect2, and RGA-3/4, J. Cell Biol. **221,** e202203017 (2022).

[23] J. F. Joanny, K. Kruse, J. Prost, and S. Ramaswamy, The actin cortex as an active wetting layer, Eur. Phys. J. E **36,** 52 (2013).

[24] N. Ecker and K. Kruse, Excitable actin dynamics and amoeboid cell migration, PLoS One **16,** e0246311 (2021).

[25] S. Etienne-Manneville and A. Hall, Rho GTPases in cell biology, Nature (London) **420,** 629 (2002).

[26] P. M. Müller *et al.*, Systems analysis of RhoGEF and RhoGAP regulatory proteins reveals spatially organized RAC1 signalling from integrin adhesions, Nat. Cell Biol. **22,** 498 (2020).

[27] K. Doubrovinski and K. Kruse, Cytoskeletal waves in the absence of molecular motors, Europhys. Lett. **83,** 18003 (2008).

[28] See Supplemental Material at http://link.aps.org/supplemental/10.1103/PhysRevLett.131.238401 for details on the linear stability analysis and the spatial dynamics, as well as additional figures.

[29] M. C. Cross and P. C. Hohenberg, Pattern formation outside of equilibrium, Rev. Mod. Phys. **65,** 851 (1993).

[30] J. Bezanson, A. Edelman, S. Karpinski, and V. B. Shah, Julia: A fresh approach to numerical computing, SIAM Rev. **59,** 65 (2017).

[31] L. Barberi and K. Kruse, v1.0, Barberi-Kruse-PRL-2023, 10.5281/zenodo.10209642.

[32] A. R. Champneys, Homoclinic orbits in reversible systems and their applications in mechanics, fluids and optics, Physica (Amsterdam) **D112,** 158 (1998).

[33] D. L. Jacono, A. Bergeon, and E. Knobloch, Magneto-hydrodynamic convectons, J. Fluid Mech. **687,** 595 (2011).

[34] E. Knobloch, Localized structures and front propagation in systems with a conservation law, IMA J. Appl. Math. **81,** 457 (2016).

[35] M. Herschkowitz-Kaufman and G. Nicolis, Localized spatial structures and nonlinear chemical waves in dissipative systems, J. Chem. Phys. **56,** 1890 (1972).

[36] M. Herschkowitz-Kaufman, Bifurcation analysis of non-linear reaction-diffusion equations—II. Steady state solutions and comparison with numerical simulations, Bull. Math. Biol. **37,** 589 (1975).

[37] Convective outflow from the peaks is allowed by the nonmonotonic dependency of $\pi(c)$ on c. If $\pi(c)$ has a monotonic dependence on c, like in Ref. [11], density peaks always generate convective inflow at their sides. In that case, the hydrodynamic interaction between neighboring peaks is attractive, which promotes their coalescence and destabil-izes LPs.

[38] W. J. Firth, L. Columbo, and A. J. Scroggie, Proposed resolution of theory-experiment discrepancy in homoclinic snaking, Phys. Rev. Lett. **99,** 104503 (2007).

[39] J. H. P. Dawes, Localized pattern formation with a large-scale mode: Slanted snaking, SIAM J. Appl. Dyn. Syst. **7,** 186 (2008).

[40] N. Verschueren and A. R. Champneys, Dissecting the snake: Transition from localized patterns to spike solutions, Physica (Amsterdam) **D419,** 132858 (2021).

[41] K. Kirchgässner, Wave-solutions of reversible systems and applications, J. Differ. Equations **45,** 113 (1982).

[42] M. Haragus and G. Iooss, *Local Bifurcations, Center Manifolds, and Normal Forms in Infinite-Dimensional Dynamical Systems* (Springer London, London, 2011).

[43] R. L. Devaney, Reversible diffeomorphisms and flows, Trans. Am. Math. Soc. **218**, 89 (1976).

[44] I. Hecht, D. A. Kessler, and H. Levine, Transient localized patterns in noise-driven reaction-diffusion systems, Phys. Rev. Lett. **104**, 158301 (2010).

[45] P. Thomas, A. Pranatharthi, C. Ross, and S. Srivastava, RhoC: A fascinating journey from a cytoskeletal organizer to a cancer stem cell therapeutic target, J. Exp. Clin. Cancer Res. **38**, 328 (2019).

[46] F. Hu, D. Zhu, H. Dong, P. Zhang, F. Xing, W. Li, R. Yan, J. Zhou, K. Xu, L. Pan, and J. Xu, Super-resolution microscopy reveals nanoscale architecture and regulation of podosome clusters in primary macrophages, iScience **25**, 105514 (2022).

[47] P. K. Mattila and P. Lappalainen, Filopodia: Molecular architecture and cellular functions, Nat. Rev. Mol. Cell Biol. **9**, 446 (2008).

[48] D. H. Bhatt, S. Zhang, and W.-B. Gan, Dendritic spine dynamics, Annu. Rev. Physiol. **71**, 261 (2009).